Advances in Nano Research, *Vol. 19, No. 2 (2025) 137-151*
https://doi.org/10.12989/anr.2025.19.2.137

Nonlinear vibrations of piezoelectric multi-scale hybrid nanocomposite sandwich plates with a negative Poisson ratio core

Farzad Ebrahimi*[1], Mohammad Mahinzare[2], Abbas Rastgoo[2] and Seyede Zahra Mirsadoghi[1]

[1]*Department of Mechanical Engineering, Faculty of Engineering, Imam Khomeini International University, Qazvin, Iran*
[2]*School of Mechanical Engineering, College of Engineering, University of Tehran, Tehran, Iran*

(*Received February 18, 2025, Revised August 18, 2025, Accepted August 19, 2025*)

Abstract. Smart hybrid meta-nanomaterials are realized through the integration of functionally graded graphene origami auxetic (FG-GOA), hybrid nanocomposite, with smart layers. This study applies the Higher-Order Shear Deformation Theory (HSDT) to investigate the nonlinear vibration of a novel piezo-electrically composite plate that is constructed with FG-GOA center and smart porous multi-scale hybrid nanocomposite (SPHNC), like Graphene Platelets (GPLs), Carbon Fibers (CF) and Polyvinylidene Fluoride (PVDF), for layers. To find out the equations that control the smart FG-GOA plate, the Generalized Differential Quadrature Method (GDQM) is implemented in order to solve the mathematical model of smart FG-GOA plates. In addition, the nonlinear frequency ratio and dynamic properties of the SPHNC are measured. Furthermore, the impact of the porosity parameter, the height of the FG-GOA core, and the height of the SPHNC layer have been investigated and shown in each figure.
Keywords: FG Auxetic; graphene origami; hybrid nanocomposite; nonlinear; smart GPL

1. Introduction

The natural frequencies investigation is an extremely important study that is performed on the structures that were studied by Asghari and Taati (2013). For the purpose of illustration, Jafari *et al*. (2014) have computed the oscillatory conduct of a FG shell equipped with nonlinearity factors. Additionally, Shen and Xiang (2014) conducted an investigation into the mathematically nonlinear oscillation of cylindrical plates composed of Negative Coefficient of Magnetostriction (NCM) layers and reinforced via foundations during thermal conditions. Additionally, Sundararajan *et al*. (2005) present the nonlinear oscillation of FG plates in temperature conditions. Furthermore

Furthermore, Sofiyev (2016) developed the vibrations of a FG cylindrical shell using von Karman terms. In different research, Ilkhani and Hosseini-Hashemi (2016) investigated the nonlinear frequency deviation of a circular plate made of FG material using a mathematical technique. Furthermore, Malekzadeh (2008) employed the DQM and the Mindlin theory to perform calculations for a nonlinear vibrational examination of an inclined plate. Also, the nonlinear oscillation of piezo FG plates was examined and determined by Ebrahimi and Rastgoo (2009). In a different piece of work, Shariyat *et al*. (2010) determined the wave propagation and oscillatory response of a cylindrical plate with temperature-dependent characteristics by applying the von Karman nonlinearity factors. In addition, Chen and Li (2017) suggested the kinematic and dynamic analysis of the plates and investigated their hypersonic airflow. Furthermore, researchers also presented a dynamic analysis of a FG beam utilizing von Karman factors, which derived from the Timoshenko theory. In another papers, Chen *et al*. (2017), Mahinzare *et al*. (2019a, b) demonstrated the post-buckling of FG beams that was made up of porous nanocomposite. Ebrahimi and Dabbagh (2019), in separated articles study on the elastic displacement of smart materials, they demonstrated that elastic displacement of smart materials is converted into electricity and voltage, as well as electrical energy, when weight is applied. Because of this, a lot of investigators have focused their attention on the characteristics of piezoelectric materials. Ebrahimi and Dabbagh (2017) investigated how waves move through smart materials and analyzed the results of their findings in the sample. Moreover, it's believed that the Motion Estimation and Enhancement (MEE) constitutive model could determine the impact that magnetic waves have on the resonance of the smart beam. Furthermore, Ebrahimi and Barati (2016a) showed the stability of a smart FG beam, and they found that the beam buckled in a zigzag pattern. The wave scattering of piezo-magnetic plates was examined by Ghorbanpour Arani *et al*. (2017), as well. Moreover, Ebrahimi and Barati (2016b) have suggested that the deformation of a piezoelectrically FG nanobeam is possible.

Zhang *et al*. (2021) have been concentrating their attention on this kind of construction because of the distinctive characteristics of metamaterials, such as an auxetic. An auxetic material was investigated by Yang *et al*. (2004), who discovered its characteristics and uses. Moreover, Wang *et al*. (2016) examined the advantages and disadvantages of NPR structures in addition to finding the specific characteristics that are associated with them. Quan

*Corresponding author, Ph.D.,
E-mail: febrahimy@eng.ikiu.ac.ir

ISSN: 2287-237X (Print), 2287-2388 (Online)

et al. (2020) also actively examined the interleaved plates in their research. Additionally, the sandwich plate has layers of gold and piezo material and an auxetic center in the middle. Furthermore, Nguyen and Pham (2018) examined the dynamic response of a plate that was comprised of honeycomb-shaped cores sandwiched together. Further, Ebrahimi (2024) provides practical insights into the application of smart and auxetic materials in engineering. It explores analytical and numerical methods while highlighting the impacts of various parameters on the mechanical characteristics, such as fracture resistance and acoustic response. Researchers examined the dynamic properties of CNT-reinforced nanocomposites, considering nanoparticle aggregation and varying length scale factors through the application of modified couple stress theory (MCST). In the sequence study, the nonlinear oscillation behavior of a smart hybrid composite plate made of graphene, CF, and PVDF with a dual FG-GOA structure was examined by Mahinzare *et al*. (2024a), using von Karman nonlinear factors, the analysis reveals hardening nonlinearity and explores the effects of parameters such as porosity and layer height on the plate's frequency response. Additionally, Jiang *et al*. (2017) analyzed the low-velocity effect of a composite construction containing an auxetic core. None of the aforementioned publications have performed an analysis of the piezo-electrically activated SPHNC for identifying the nonlinear resonance of the plate. This study is the initial paper that has provided the nonlinear frequency deviation of a composite plate with (HSDT). The substance that makes up this smart multi-scale hybrid nanocomposite metamaterial consists of permeable layers of (GPL/CF/PVDF) and a FG-GOA core. In addition, the formulas that control this sandwich plate are obtained. Through the use of the GDQM, these controlling equations are given a discrete form. It is possible to demonstrate that the height of the SPHNC layer, the height of the FG-GOA core, the external voltage, and the weight percentage of GPL have all contributed to the (ω_{NL}/ω) ratio of the piezoelectrically controlled plate. The examined problem is important because understanding the nonlinear vibrations of piezoelectric multi-scale hybrid nanocomposite sandwich plates with an auxetic core is crucial for the design of advanced smart materials and structures. Such structures, integrating graphene origami auxetic cores with multi-scale hybrid nanocomposite layers, offer enhanced mechanical performance, energy absorption, and vibration control. Addressing this problem not only advances the fundamental knowledge of smart meta-nanomaterials but also provides valuable insights for applications in actuators, flexible electronics, and adaptive engineering systems.

2. The formulation

2.1 Material properties

2.1.1 SPHNC layer

Via utilizing the Halpin-Tsai (HT) model and the Rules of Mixture (ROM), the calculated effective characteristics of the GPL are reported. According to the assumptions made in this article, the uniform pattern of GPL looks like

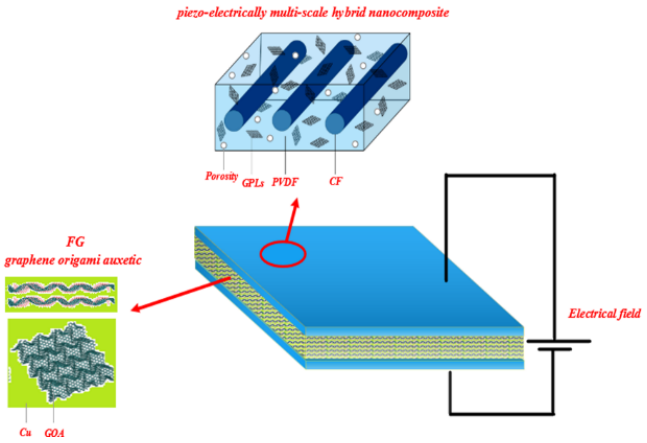

Fig. 1 (a) The diagram of the SPHNC sandwich plate containing a FG-GOA core

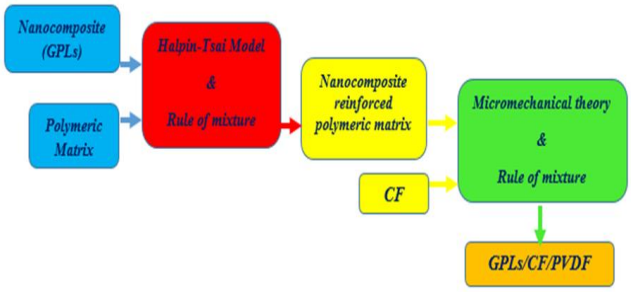

Fig. 1 (b) Combining procedure of GPLs/CF/PVDF piezo-electrically SPHNC

Fig. 1(a,b):

$$W_{GPL} = 100 W_C W_{GPL}^t \tag{1.1}$$

where W_C and W_{GPL}^t denote the unique property of the nanoplatelets of graphene and their percentage by weight, correspondingly.

Finding the volume percentage of nanoplatelets of graphene can be done as below:

$$V_{GPL} = \frac{W_{GPL}}{W_{GPL} + \left(\frac{\rho_{GPL}}{\rho_M}\right)(1 - W_{GPL})} \tag{1.2}$$

ρ_{GPL} and ρ_M represent the relative concentrations of nanoplatelets comprised of graphene and (PVDF) matrix, respectively.

Using the Halpin-Tsai model, the effective elasticity of SNCM can be calculated as described below:

$$E_{SNCM} = \left(\frac{3}{8}E_L + \frac{5}{8}E_T\right) \tag{1.3}$$

In which (E_L) and (E_T) denote the longitudinal and transverse modulus of the SNC correspondingly.

$$\{E_L, E_T\} = \left\{\frac{1 + \xi_L^{GPL}\eta_L^{GPL}V_{GPL}}{1 - \eta_L^{GPL}V_{GPL}}, \frac{1 + \xi_W^{GPL}\eta_W^{GPL}V_{GPL}}{1 - \eta_W^{GPL}V_{GPL}}\right\}E_M \tag{1.4}$$

$$\{\eta_L^{GPL}, \eta_W^{GPL}\} = \left\{\frac{\left(\frac{E_{GPL}}{E_M}\right) - 1}{\left(\frac{E_{GPL}}{E_M}\right) + \xi_L^{GPL}}, \frac{\left(\frac{E_{GPL}}{E_M}\right) - 1}{\left(\frac{E_{GPL}}{E_M}\right) + \xi_W^{GPL}}\right\}$$
$$\{\xi_L^{GPL}, \xi_W^{GPL}\} = \left\{\frac{2l_{GPL}}{t_{GPL}}, \frac{2w_{GPL}}{t_{GPL}}\right\} \tag{1.5}$$

in which the dimensions of the graphene are represented by the symbols l_{GPL}, w_{GPL}, and t_{GPL} for length, breadth, and height, respectively; additionally, the Poisson's ratio, density, dielectric, and piezoelectric constants of the SNC layer can be calculated utilizing the rule of mixtures ROM. These values can be found as follows:

$$V_{GPL} + V_M = 1 \tag{1.6}$$

$$\rho_{SNC} = (V_M \rho^M + V_{GPL} \rho^{GPL}) \tag{1.7}$$

$$\nu_{SNC} = V_M \nu^M + V_{GPL} \nu^{GPL} \tag{1.8}$$

$$G_{SNC} = \left(\frac{E_{SNC}}{2(1+\nu_{SNC})}\right) \tag{1.9}$$

$$e_{ij}^{SNC} = V_M {e_{ij}}^M + V_{GPL} e_{ij}^{GPL} \tag{1.10}$$

$$s_{ij}^{SNC} = V_M {s_{ij}}^M + V_{GPL} s_{ij}^{GPL} \tag{1.11}$$

Carbon fiber CF and GPL are used to strengthen the sections of the smart hybrid nanocomposite SHNC. Instead, we can observe the following useful characteristics of the mixed nanocomposite layers:

$$V_{SNC} + V_F = 1 \tag{1.12}$$

$$E_{SHNC} = (V_{SNC} E^{SNC} + V_F E^F) \tag{1.13}$$

$$\rho_{SHNC} = (V_{SNC} \rho^{SNC} + V_F \rho^F) \tag{1.14}$$

$$\nu_{SHNC} = (V_{SNC} \nu^{SNC} + V_F \nu^F) \tag{1.15}$$

$$G_{SHNC} = \left(\frac{E_{SHNC}}{2(1+\nu_{SHNC})}\right) \tag{1.16}$$

$$e_{ij}^{SHNC} = \left(V_{SNCM} e_{ij}^{SNC} + V_F e_{ij}^F\right) \tag{1.17}$$

$$s_{ij}^{SHNC} = \left(V_{SNCM} s_{ij}^{SNC} + V_F s_{ij}^F\right) \tag{1.18}$$

Then, we can calculate the following as an approximation of the characteristics of a SPHNC, Where F signified fibers, the following formulas are adapted from the homogenization models proposed by (Mahinzare *et al*. 2024b) where the porosity coefficient (e_0) and correction function (λ) are introduced to account for the influence of porous on stiffness and density. These expressions have been successfully employed in recent studies on porous hybrid nanocomposites and provide a reliable approximation for characterizing SPHNC materials:

$$E_{SPHNC} = E_{SHNC}(1 - e_0\lambda) \tag{1.19}$$

$$G_{SPHNC} = G_{SHNC}(1 - e_0\lambda) \tag{1.20}$$

$$\rho_{SPHNC} = \rho_{SHNC}\left(\sqrt{1 - e_0\lambda}\right) \tag{1.21}$$

where SPHNC indicated the smart porous hybrid nanocomposite similar to how (e_0) stands for permeability, (e_m) signifies mass density.

$$e_m = 1 - \sqrt{1 - e_0} \tag{1.22}$$

It's additionally possible to give the following definitive forms:

$$\lambda = \frac{1}{e_0} - \frac{1}{e_0}\left\{\frac{2}{\pi}\sqrt{1 - e_0} - \frac{2}{\pi} + 1\right\}^2 \tag{1.23}$$

2.1.2 FG-GOA core

Moreover, the given characteristics of GOA would be derived by:

$$E^{Auxetic} = E_{Cu}\frac{1 + \xi\eta V_{Gr}}{1 - \eta V_{Gr}} f_E(H_{Gr}, V_{Gr}, T) \tag{2.1}$$

$$\nu^{Auxetic} = (V_{Gr}\nu_{Gr} + V_{Cu}\nu_{Cu}) f_\nu(H_{Gr}, V_{Gr}, T) \tag{2.2}$$

$$\alpha^{Auxetic} = (V_{Gr}\alpha_{Gr} + V_{Cu}\alpha_{Cu}) f_\alpha(V_{Gr}, T) \tag{2.3}$$

$$\rho^{Auxetic} = (V_{Gr}\rho_{Gr} + V_{Cu}\rho_{Cu}) f_\rho(V_{Gr}, T) \tag{2.4}$$

$$\begin{aligned}
f_E(H_{Gr}, V_{Gr}, T) &= \begin{pmatrix} 1.11 - 1.22V_{Gr} - 0.134\left(\frac{T}{T_0}\right) \\ +0.559V_{Gr}\left(\frac{T}{T_0}\right) - 5.5H_{Gr}V_{Gr} \\ +38H_{Gr}V_{Gr}^2 - 20.6H_{Gr}^2V_{Gr}^2 \end{pmatrix} \\
f_\nu(H_{Gr}, V_{Gr}, T) &= \begin{pmatrix} 1.01 - 1.43V_{Gr} + 0.165\left(\frac{T}{T_0}\right) \\ -16.8H_{Gr}V_{Gr} - 1.1H_{Gr}V_{Gr}\left(\frac{T}{T_0}\right) \\ +16H_{Gr}^2V_{Gr}^2 \end{pmatrix} \\
f_\alpha(V_{Gr}, T) &= \begin{pmatrix} 0.794 - 16.8V_{Gr}^2 - 0.0279\left(\frac{T}{T_0}\right)^2 \\ +0.182\left(\frac{T}{T_0}\right)(V_{Gr} + 1) \end{pmatrix} \\
f_\rho(V_{Gr}, T) &= \left(1.01 - 2.01V_{Gr}^2 - 0.0131\left(\frac{T}{T_0}\right)\right)
\end{aligned} \tag{2.5}$$

The weight proportion of graphene origami is represented by W_{Gr} and Cu is represented by $V_{Gr} = \frac{\rho_{Cu}W_{Gr}}{\rho_{Cu}W_{Gr} + \rho_{Gr}(1 - W_{Gr})}, V_{Cu} = 1 - V_{Gr}$, both of which $f_{E,\nu,\alpha,\rho}(H_{Gr}, V_{Gr}, T)$ can be identified using MD, making them useful indicators of both material and dimension constants $\eta = \frac{\frac{E_{Gr}}{E_{Cu}} - 1}{\frac{E_{Gr}}{E_{Cu}} + \xi}, \xi = 2\left(\frac{l_{Gr}}{t_{Gr}}\right)$ FG- Auxetic Models, Moreover, the resulting form can be used to discover the characteristics of the FG-GOA with the following distinct FG distributions:

$$V_{Gr}(z) = V_{Gr}\left|\frac{4z}{h_{FG-GOA}}\right|^n \tag{2.6}$$

2.2 Constitutive model

The following formulae derive from the electro-elastic mathematical model of the composite plate

Based on articles by Mahinzare *et al*. (2024) and Ebrahimi and Barati (2016c):

$$\sigma_{ij} = \left[C_{ijkl}\varepsilon_{kl} - e_{mij}E_m\right],\ D_i = \left[e_{ikl}\varepsilon_{kl} + s_{im}E_m\right] \quad (3)$$

In which C_{ijkl}, σ_{ij}-ε_{kl} are stand for the components of the stress - strain matrix. Furthermore, D_i and E_m designated for the electrical motion and electric potential components, correspondingly. Both s_{im}ande_{ikl} denote the dielectric and piezoelectric coefficients, correspondingly. Accordingly, the smart plate's stress-strain equation can be shown as:

$$\begin{Bmatrix}\sigma_{xx}\\ \sigma_{yy}\\ \sigma_{yz}\\ \sigma_{zx}\\ \sigma_{xy}\end{Bmatrix} = \left\{\begin{pmatrix} c_{11} & c_{12} & 0 & 0 & 0\\ c_{12} & c_{11} & 0 & 0 & 0\\ 0 & 0 & c_{55} & 0 & 0\\ 0 & 0 & 0 & c_{55} & 0\\ 0 & 0 & 0 & 0 & c_{66}\end{pmatrix}\begin{Bmatrix}\varepsilon_{xx}\\ \varepsilon_{yy}\\ \varepsilon_{yz}\\ \varepsilon_{zx}\\ \varepsilon_{xy}\end{Bmatrix} - \begin{pmatrix} 0 & 0 & e_{31}\\ 0 & 0 & e_{31}\\ 0 & e_{15} & 0\\ e_{15} & 0 & 0\\ 0 & 0 & 0\end{pmatrix}\begin{Bmatrix}E_x\\ E_y\\ E_z\end{Bmatrix}\right\}$$

$$\begin{Bmatrix}D_x\\ D_y\\ D_z\end{Bmatrix} = \left\{\begin{pmatrix} 0 & 0 & 0 & 0 & e_{15} & 0\\ 0 & 0 & 0 & e_{15} & 0 & 0\\ e_{31} & e_{31} & 0 & 0 & 0 & 0\end{pmatrix}\begin{Bmatrix}\varepsilon_{xx}\\ \varepsilon_{yy}\\ \varepsilon_{zz}\\ \varepsilon_{yz}\\ \varepsilon_{zx}\\ \varepsilon_{xy}\end{Bmatrix} + \begin{pmatrix} s_{11} & 0 & 0\\ 0 & s_{11} & 0\\ 0 & 0 & s_{33}\end{pmatrix}\begin{Bmatrix}E_x\\ E_y\\ E_z\end{Bmatrix}\right\} \quad (4)$$

2.3 Kinematics relations

HSDT provides the subsequent expression of the displacement of the composite plate:

$$U(x,y,z,t) = u(x,y,t) - z\frac{\partial w(x,y,t)}{\partial x} + Z(z)\left(\psi_x(x,y,t) + \frac{\partial w(x,y,t)}{\partial x}\right) \quad (5.1)$$

$$V(x,y,z,t) = v(x,y,t) - z\frac{\partial w(x,y,t)}{\partial x} + Z(z)\left(\psi_y(x,y,t) + \frac{\partial w(x,y,t)}{\partial x}\right) \quad (5.2)$$

$$W(x,y,z,t) = w(x,y,t), \qquad Z(z) = \left(z - \frac{4z^3}{3h^2}\right) \quad (5.3)$$

In which, u_0 represents the longitudinal displacement, v_0 signifies the transverse displacement, and w represents the horizontal deviation of the sandwich plate. Furthermore, ψ_x and ψ_y indicated transverse normal revolutions along axes x and y.

The following formulae are used to predict the conditions in which, by Maxwell's law would be satisfied:

$$\Phi(x,y,z,t) = -cos(\zeta z)\phi(x,z,t) + \frac{2z}{h}V_0 \quad (6)$$

That $\zeta = \frac{\pi}{h}$.

Where V_0 stands for the electrical power from the outside environment. Furthermore, the sandwich plate stresses can be accomplished as:

$$\begin{Bmatrix}\varepsilon_{xx}\\ \varepsilon_{yy}\\ \varepsilon_{xy}\end{Bmatrix} = \begin{Bmatrix}\varepsilon^0_{xx}\\ \varepsilon^0_{yy}\\ \varepsilon^0_{xy}\end{Bmatrix} + z\begin{Bmatrix}k^b_{xx}\\ k^b_{yy}\\ k^b_{xy}\end{Bmatrix}, \begin{Bmatrix}\gamma_{xz}\\ \gamma_{yz}\end{Bmatrix} = \begin{Bmatrix}\gamma^0_{xz}\\ \gamma^0_{yz}\end{Bmatrix} \quad (7.1)$$

$$Z_1 = Z(z) - z, \qquad Z_2 = Z(z), \qquad Z_3 = \frac{dZ(z)}{dz} \quad (7.2)$$

Piezoelectrically actuated plate von Karman strain can be calculated using the following equation:

$$\begin{Bmatrix}\varepsilon^0_{xx}\\ \varepsilon^0_{yy}\\ \varepsilon^0_{xy}\end{Bmatrix} = \begin{Bmatrix}\frac{\partial u}{\partial x} + \frac{1}{2}\left(\frac{\partial w}{\partial x}\right)^2\\ \frac{\partial v}{\partial x} + \frac{1}{2}\left(\frac{\partial w}{\partial y}\right)^2\\ \frac{\partial u}{\partial y} + \frac{\partial v}{\partial x} + \frac{\partial w}{\partial x}\frac{\partial w}{\partial y}\end{Bmatrix},$$

$$\begin{Bmatrix}k^b_{xx}\\ k^b_{yy}\\ k^b_{xy}\end{Bmatrix} = \begin{Bmatrix}-\frac{\partial^2 w}{\partial x^2}\\ -\frac{\partial^2 w}{\partial y^2}\\ -\frac{\partial^2 w}{\partial x \partial y}\end{Bmatrix}, \begin{Bmatrix}k^s_{xx}\\ k^s_{yy}\\ k^s_{xy}\end{Bmatrix} = \begin{Bmatrix}\frac{\partial \psi_x}{\partial x}\\ \frac{\partial \psi_y}{\partial y}\\ \frac{\partial \psi_x}{\partial y} + \frac{\partial \psi_y}{\partial x}\end{Bmatrix}, \quad (8)$$

$$\begin{Bmatrix}\gamma^0_{xz}\\ \gamma^0_{yz}\end{Bmatrix} = \begin{Bmatrix}\frac{\partial w}{\partial x} + \psi_x\\ \frac{\partial w}{\partial y} + \psi_y\end{Bmatrix}$$

Also, the sandwich plate's electrical fields could be performed in the following ways:

$$E_x = -\frac{\partial \Phi}{\partial x} = cos(\zeta z)\frac{\partial \phi}{\partial x},$$
$$E_y = -\frac{\partial \Phi}{\partial y} = cos(\zeta z)\frac{\partial \phi}{\partial y}, \quad (9)$$
$$E_z = -\frac{\partial \Phi}{\partial z} = -\zeta\, sin(\zeta z)\phi - \frac{2V_E}{h}$$

Applying Hamilton's principle to a piezoelectrically activated plate results in the aforementioned shape being used to describe the concept:

$$\int_0^t \delta(\Pi_S - \Pi_K + \Pi_W)dt = 0 \quad (10)$$

The strain as well as kinetic energy are represented by Π_S and Π_K correspondingly. In addition, the labor done by the smart plate's exterior is represented by Π_W the sign. In addition to this, the strain energy can indeed be performed by:

$$\begin{aligned}\Pi_S &= \int_V (\sigma_{ij}\varepsilon_{ij})dV \\ &= \int_V \begin{pmatrix}\sigma_{xx}\varepsilon_{xx}+\sigma_{yy}\varepsilon_{yy}+\sigma_{xy}\varepsilon_{xy}+\sigma_{xz}\varepsilon_{xz}\\ +\sigma_{yz}\varepsilon_{yz}-D_xE_x-D_yE_y-D_zE_z\end{pmatrix}dV\end{aligned} \quad (11)$$

Following Eqs. (5-7) into Eq.(9) would yield the strain energy below:

$$\begin{aligned}\Pi_S &= \int_A \begin{pmatrix}N_{xx}\varepsilon^0_{xx}+M_{xx}\varepsilon^1_{xx}+P_{xx}\varepsilon^2_{xx}\\ +N_{yy}\varepsilon^0_{yy}+M_{yy}\varepsilon^1_{yy}+P_{yy}\varepsilon^2_{xx}\\ +2N_{xy}\varepsilon^0_{xy}+2M_{xy}\varepsilon^1_{xy}+2P_{xy}\varepsilon^2_{xy}\\ +Q_{xz}\gamma^0_{xz}+Q_{yz}\gamma^0_{yz}\end{pmatrix}dA \\ &+\int_{-h/2}^{h/2}\int_A \Big(-D_x\cos(\zeta z)\delta(\frac{\partial\phi}{\partial x})-D_y\cos(\zeta z)\delta(\frac{\partial\phi}{\partial y}) \\ &\quad +D_z\sin(\zeta z)\delta\phi\Big)dAdz\end{aligned} \quad (12)$$

Obtaining the force and moment exerted by the sandwich plate by using the following equations:

$$(N_{xx}, N_{yy}, N_{xy}) = \quad (13)$$

Furthermore, External work is described as:

$$\delta\Pi_W = \frac{1}{2}\int_A \left(N_x^E\left(\frac{\partial w}{\partial x}\right)^2 + N_y^E\left(\frac{\partial w}{\partial y}\right)^2\right)dA \quad (14)$$

where N_x^E and N_y^E indicated the exterior electrical activity in the x and y directions in that order. Furthermore, the following methods can be used to acquire the kinetic energy:

$$\Pi_K = \frac{1}{2}\int_A \begin{pmatrix} I_0\left(\frac{\partial u}{\partial t}\right)^2 + I_0\left(\frac{\partial v}{\partial t}\right)^2 \\ +I_0\left(\frac{\partial w}{\partial t}\right)^2 + I_3\left(\frac{\partial \psi_x}{\partial t}\right)^2 + I_3\left(\frac{\partial \psi_y}{\partial t}\right)^2 \\ +I_1\left[\left(\frac{\partial^2 w}{\partial t\partial x}\right)^2 + \left(\frac{\partial^2 w}{\partial t\partial y}\right)^2\right] \\ +2I_2\left[\frac{\partial\psi_x}{\partial t}\frac{\partial^2 w}{\partial t\partial x}+\frac{\partial\psi_y}{\partial t}\frac{\partial^2 w}{\partial t\partial y}\right]\end{pmatrix}dA \quad (15)$$

The mass inertias can be calculated as shown below:

$$(I_0, I_1, I_2, I_3) = \int_{-h/2}^{h/2}(1, Z_1^2, Z_1Z_2, Z_2^2)\rho(z)dz \quad (16)$$

In order to write sandwich plate equations of motion, you would need to replace Eqs. (10), (13), and Eq. (14) with Eq. (8).

$$\frac{\partial N_{xx}}{\partial x}+\frac{\partial N_{xy}}{\partial y} = I_0\frac{\partial^2 u}{\partial t^2} \quad (17.1)$$

$$\frac{\partial N_{xy}}{\partial x}+\frac{\partial N_{yy}}{\partial y} = I_0\frac{\partial^2 v}{\partial t^2} \quad (17.2)$$

$$\begin{aligned}&\frac{\partial}{\partial x}\left(N_{xx}\frac{\partial w}{\partial x}+N_{xy}\frac{\partial w}{\partial y}\right)+\frac{\partial}{\partial y}\left(N_{xy}\frac{\partial w}{\partial x}+N_{yy}\frac{\partial w}{\partial y}\right) \\ &+\frac{\partial Q_{xz}}{\partial x}+\frac{\partial Q_{yz}}{\partial y}-\frac{\partial^2 P_{xx}}{\partial x^2}-\frac{\partial^2 P_{xy}}{\partial x\partial y}-\frac{\partial^2 P_{yy}}{\partial y^2}-N^E\nabla^2 w \\ &= I_0\frac{\partial^2 w}{\partial t^2}-I_1\left(\frac{\partial^4 w}{\partial t^2\partial x^2}+\frac{\partial^4 w}{\partial t^2\partial y^2}\right) \\ &\quad +I_2\left(\frac{\partial^3\psi_x}{\partial t^2\partial x}+\frac{\partial^3\psi_y}{\partial t^2\partial y}\right)\end{aligned} \quad (17.3)$$

$$\frac{\partial M_{xx}}{\partial x}+\frac{\partial M_{xy}}{\partial y}-Q_{xz} = I_3\frac{\partial^2\psi_x}{\partial t^2}+I_2\frac{\partial^3 w}{\partial t^2\partial x} \quad (17.4)$$

$$\frac{\partial M_{xy}}{\partial x}+\frac{\partial M_{yy}}{\partial y}-Q_{yz} = I_3\frac{\partial^2\psi_y}{\partial t^2}+I_2\frac{\partial^3 w}{\partial t^2\partial y} \quad (17.5)$$

$$\int_A\left(\cos(\zeta z)\frac{\partial D_x}{\partial x}+\cos(\zeta z)\frac{\partial D_y}{\partial y}+\zeta\sin(\zeta z)D_z\right)dA \quad (17.6)$$

The calculated forces and moments are presented as per the constitutive equations:

$$\begin{Bmatrix}N_{xx}\\N_{yy}\\N_{xy}\end{Bmatrix} = \begin{pmatrix}\begin{pmatrix}A_{11}&A_{12}&0\\A_{21}&A_{22}&0\\0&0&A_{66}\end{pmatrix}\begin{Bmatrix}\frac{\partial u}{\partial x}+\frac{1}{2}\left(\frac{\partial w}{\partial x}\right)^2\\ \frac{\partial v}{\partial x}+\frac{1}{2}\left(\frac{\partial w}{\partial y}\right)^2\\ \frac{\partial u}{\partial y}+\frac{\partial v}{\partial x}+\frac{\partial w}{\partial x}\frac{\partial w}{\partial y}\end{Bmatrix} \\ +\begin{pmatrix}A_{31}\\A_{31}\\0\end{pmatrix}\phi-\begin{pmatrix}N_x^E\\N_y^E\\0\end{pmatrix}\end{pmatrix} \quad (18)$$

$$\begin{Bmatrix}M_{xx}\\M_{yy}\\M_{xy}\end{Bmatrix} = \begin{pmatrix}\begin{pmatrix}C_{11}&C_{12}&0\\C_{21}&C_{22}&0\\0&0&C_{66}\end{pmatrix}\begin{Bmatrix}\frac{\partial^2 w}{\partial x^2}\\ \frac{\partial^2 w}{\partial y^2}\\ \frac{\partial^2 w}{\partial x\partial y}\end{Bmatrix}+ \\ \begin{pmatrix}D_{11}&D_{12}&0\\D_{21}&D_{22}&0\\0&0&D_{66}\end{pmatrix}\begin{Bmatrix}\frac{\partial\psi_x}{\partial x}\\ \frac{\partial\psi_y}{\partial y}\\ \frac{\partial\psi_x}{\partial y}+\frac{\partial\psi_y}{\partial x}\end{Bmatrix}+\begin{pmatrix}E_{31}\\E_{31}\\0\end{pmatrix}\phi-\begin{pmatrix}M_x^E\\M_y^E\\0\end{pmatrix}\end{pmatrix} \quad (19)$$

$$\begin{Bmatrix}P_{xx}\\P_{yy}\\P_{xy}\end{Bmatrix} = \begin{pmatrix}\begin{pmatrix}D_{11}&D_{12}&0\\D_{21}&D_{22}&0\\0&0&D_{66}\end{pmatrix}\begin{Bmatrix}\frac{\partial^2 w}{\partial x^2}\\ \frac{\partial^2 w}{\partial y^2}\\ \frac{\partial^2 w}{\partial x\partial y}\end{Bmatrix}+ \\ \begin{pmatrix}H_{11}&H_{12}&0\\H_{21}&H_{22}&0\\0&0&H_{66}\end{pmatrix}\begin{Bmatrix}\frac{\partial\psi_x}{\partial x}\\ \frac{\partial\psi_y}{\partial y}\\ \frac{\partial\psi_x}{\partial y}+\frac{\partial\psi_y}{\partial x}\end{Bmatrix}+\begin{pmatrix}G_{31}\\G_{31}\\0\end{pmatrix}\phi-\begin{pmatrix}M_x^E\\M_y^E\\0\end{pmatrix}\end{pmatrix} \quad (20)$$

$$\begin{Bmatrix}Q_{xz}\\Q_{yz}\end{Bmatrix} = \left(\begin{pmatrix}A_{44}&0\\0&A_{55}\end{pmatrix}\begin{Bmatrix}\frac{\partial w}{\partial x}+\psi_x\\ \frac{\partial w}{\partial y}+\psi_y\end{Bmatrix}-E_{15}\begin{Bmatrix}\frac{\partial\phi}{\partial x}\\ \frac{\partial\phi}{\partial y}\end{Bmatrix}\right) \quad (21)$$

$$\int_A\left(\begin{Bmatrix}D_x\\D_y\end{Bmatrix}\cos(\zeta z)\right)dA = \left(E_{15}\begin{Bmatrix}\frac{\partial w}{\partial x}+\psi_x\\ \frac{\partial w}{\partial y}+\psi_y\end{Bmatrix}+X_{11}\begin{Bmatrix}\frac{\partial\phi}{\partial x}\\ \frac{\partial\phi}{\partial y}\end{Bmatrix}\right) \quad (22)$$

$$\int_A (D_z\,\zeta\,sin(\zeta\,z))\,dA = \begin{pmatrix} E_{31}\left(\frac{\partial^2 w}{\partial x^2}+\frac{\partial^2 w}{\partial y^2}\right) \\ G_{31}\left(\frac{\partial \psi_x}{\partial x}+\frac{\partial \psi_y}{\partial y}\right) - X_{33}\phi \end{pmatrix} \quad (23)$$

where:

$$\begin{bmatrix} A_{11} & D_{11} & C_{11} & H_{11} \\ A_{12} & D_{12} & C_{12} & H_{12} \\ A_{66} & D_{66} & C_{66} & H_{66} \\ A_{44} & D_{44} & C_{44} & H_{44} \\ A_{55} & D_{55} & C_{55} & H_{55} \end{bmatrix} = \begin{pmatrix} (1, Z_1 Z_2, Z_1^2, Z_2^2) \left\{ 2\int_{\frac{-h}{2}}^{-\frac{h}{2}+h_{SPHNC}} \begin{Bmatrix} c_{11}^{SHNC} \\ c_{12}^{SHNC} \\ c_{66}^{SHNC} \\ c_{44}^{SHNC} \\ c_{55}^{SHNC} \end{Bmatrix} dz \right. \\ \left. + \int_{-h_{FG-GOA}/2}^{h_{FG-GOA}/2} \begin{Bmatrix} c_{11}^{FG-GOA} \\ c_{12}^{FG-GOA} \\ c_{66}^{FG-GOA} \\ c_{44}^{FG-GOA} \\ c_{55}^{FG-GOA} \end{Bmatrix} dz \right\} \end{pmatrix} \quad (24)$$

$$E_{31} = 2\int_{-\frac{h}{2}}^{-\frac{h}{2}+h_{SPHNC}} e_{31}\zeta\,sin(\zeta z) Z_1 dz\,,$$

$$G_{31} = 2\int_{-\frac{h}{2}}^{-\frac{h}{2}+h_{SPHNC}} e_{31}\zeta\,sin(\zeta z) Z_2 dz$$

$$E_{15} = 2\int_{-\frac{h}{2}}^{-\frac{h}{2}+h_{SPHNC}} e_{15}\,cos(\zeta z) Z_3 dz\,, \quad (25)$$

$$\{X_{11}, Y_{11}\} = 2\int_{-h/2}^{-\frac{h}{2}+h_{SPHNC}} \{s_{11}, d_{11}\}\,cos^2(\zeta z) Z_3 dz$$

$$\{X_{33}, Y_{33}\} = 2\int_{-h/2}^{-\frac{h}{2}+h_{SPHNC}} \{s_{33}, d_{33}\}\zeta^2\,sin^2(\zeta z) dz$$

In addition, the externally applied electric voltage generates forces and moments influenced by external electrical activity, which will be expressed as follows:

$$N^E = N_x^E = N_y^E = -2\int_{-h/2}^{-\frac{h}{2}+h_{SPHNC}} \left(e_{31}\frac{2V_0}{h_{SPHNC}}\right) dz \quad (26)$$

$$M^E = M_x^E = M_y^E = -2\int_{-\frac{h}{2}}^{-\frac{h}{2}+h_{SHNC}} \left(e_{31}\frac{2V_0}{h_{SPHNC}}\right) z dz \quad (27)$$

It is feasible to obtain the nonlinear equations of the piezoelectrically used plate in the subsequent forms by inserting Eqs. (18)-(24) into Eqs. (17.1)-(17.7).

$$\begin{pmatrix} A_{11}\left(\frac{\partial^2 u}{\partial x^2}+\frac{\partial w}{\partial x}\frac{\partial^2 w}{\partial x^2}\right) \\ +(A_{12}+A_{66})\left(\frac{\partial^2 v}{\partial x \partial y}+\frac{\partial w}{\partial y}\frac{\partial^2 w}{\partial x \partial y}\right) \\ +A_{66}\left(\frac{\partial^2 u}{\partial y^2}+\frac{\partial w}{\partial x}\frac{\partial^2 w}{\partial y^2}\right) \end{pmatrix} = I_0\frac{\partial^2 u_0}{\partial t^2} \quad (28.1)$$

$$\begin{pmatrix} A_{22}\left(\frac{\partial^2 v}{\partial y^2}+\frac{\partial w}{\partial y}\frac{\partial^2 w}{\partial y^2}\right) \\ +(A_{12}+A_{66})\left(\frac{\partial^2 u}{\partial x \partial y}+\frac{\partial w}{\partial x}\frac{\partial^2 w}{\partial x \partial y}\right) \\ +A_{66}\left(\frac{\partial^2 v}{\partial x^2}+\frac{\partial w}{\partial y}\frac{\partial^2 w}{\partial x^2}\right) \end{pmatrix} = I_0\frac{\partial^2 v}{\partial t^2} \quad (28.2)$$

$$\begin{pmatrix} k_s A_{44}\left(\frac{\partial^2 w}{\partial x^2}+\frac{\partial^2 w}{\partial y^2}+\frac{\partial \psi_x}{\partial x}+\frac{\partial \psi_y}{\partial y}\right) \\ -(k_s E_{15}+E_{31})\left(\frac{\partial^2 \phi}{\partial x^2}+\frac{\partial^2 \phi}{\partial y^2}\right) \\ -C_{11}\frac{\partial^4 w}{\partial x^4} - 2(C_{12}-2C_{11})\frac{\partial^4 w}{\partial x^2 \partial y^2} \\ -C_{22}\frac{\partial^4 w}{\partial y^4} - D_{11}\frac{\partial^3 \psi_x}{\partial x^3} \\ -(D_{12}+2D_{66})\left(\frac{\partial^3 \psi_x}{\partial x \partial x^2}+\frac{\partial^3 \psi_y}{\partial x^2 \partial y}\right) - D_{22}\frac{\partial^3 \psi_y}{\partial y^3} \\ +N^E\left(\frac{\partial^2 w}{\partial x^2}+\frac{\partial^2 w}{\partial y^2}\right)+Z_1+Z_2 \end{pmatrix} = \begin{pmatrix} I_0\frac{\partial^2 w}{\partial t^2} \\ -I_1\left(\frac{\partial^4 w}{\partial t^2 \partial x^2}+\frac{\partial^4 w}{\partial t^2 \partial y^2}\right) \\ +I_2\left(\frac{\partial^3 \psi_x}{\partial t^2 \partial x}+\frac{\partial^3 \psi_x}{\partial t^2 \partial y}\right) \end{pmatrix} \quad (28.3)$$

$$\begin{pmatrix} +(G_{31}+k_s E_{15})\frac{\partial \phi}{\partial x}+(L_{31}+k_s Q_{15})\frac{\partial \psi}{\partial x} \\ -k_s A_{44}\left(\frac{\partial w}{\partial x}+\psi_x\right)+D_{11}\frac{\partial^3 w}{\partial x^3} \\ +(D_{12}+2D_{66})\frac{\partial^3 w}{\partial x \partial y^2}+H_{11}\frac{\partial^3 \psi_x}{\partial x^3} \\ +(H_{12}+H_{66})\frac{\partial^2 \psi_y}{\partial x \partial y}+H_{66}\frac{\partial^3 \psi_x}{\partial y^3} \end{pmatrix} = \left(I_3\frac{\partial^2 \psi_x}{\partial t^2}+I_2\frac{\partial^3 w}{\partial t^2 \partial x}\right) \quad (28.4)$$

$$\begin{pmatrix} +(G_{31}+k_s E_{15})\frac{\partial \phi}{\partial x}+(L_{31}+k_s Q_{15})\frac{\partial \psi}{\partial x} \\ -k_s A_{44}\left(\frac{\partial w}{\partial y}+\psi_y\right)+D_{22}\frac{\partial^3 w}{\partial y^3} \\ +(D_{12}+2D_{66})\frac{\partial^3 w}{\partial x^2 \partial y}+H_{66}\frac{\partial^2 \psi_y}{\partial x^2} \\ +(H_{12}+H_{66})\frac{\partial^2 \psi_x}{\partial x \partial y}+H_{22}\frac{\partial^2 \psi_y}{\partial y^2} \end{pmatrix} = \left(I_3\frac{\partial^2 \psi_y}{\partial t^2}+I_2\frac{\partial^3 w}{\partial t^2 \partial y}\right) \quad (28.5)$$

$$\begin{pmatrix} E_{15}\left(\frac{\partial^2 w}{\partial x^2}+\frac{\partial^2 w}{\partial y^2}+\frac{\partial \psi_x}{\partial x}+\frac{\partial \psi_y}{\partial y}\right) \\ +G_{31}\left(\frac{\partial \psi_x}{\partial x}+\frac{\partial \psi_y}{\partial y}\right)+X_{11}\left(\frac{\partial^2 \phi}{\partial x^2}+\frac{\partial^2 \phi}{\partial y^2}\right) \\ +E_{31}\left(\frac{\partial^2 w}{\partial x^2}+\frac{\partial^2 w}{\partial y^2}\right)-X_{33}\phi \end{pmatrix} = 0 \quad (28.6)$$

$$
\begin{aligned}
Z_1 = &\begin{bmatrix} A_{11}\left(\frac{\partial u}{\partial x}+\frac{1}{2}\left(\frac{\partial w}{\partial x}\right)^2\right) \\ +A_{12}\left(\frac{\partial v}{\partial y}+\frac{1}{2}\left(\frac{\partial w}{\partial y}\right)^2\right)\end{bmatrix}\left(\frac{\partial^2 w}{\partial x^2}\right) \\
&+\begin{bmatrix} A_{11}\left(\frac{\partial^2 u}{\partial x^2}+\frac{\partial w}{\partial x}\frac{\partial^2 w}{\partial x^2}\right) \\ +A_{12}\left(\frac{\partial^2 v}{\partial x\partial y}+\frac{\partial w}{\partial y}\frac{\partial^2 w}{\partial x\partial y}\right)\end{bmatrix}\left(\frac{\partial w}{\partial x}\right) \\
&+\begin{bmatrix} A_{12}\left(\frac{\partial u}{\partial x}+\frac{1}{2}\left(\frac{\partial w}{\partial x}\right)^2\right) \\ +A_{11}\left(\frac{\partial v}{\partial y}+\frac{1}{2}\left(\frac{\partial w}{\partial y}\right)^2\right)\end{bmatrix}\left(\frac{\partial^2 w}{\partial y^2}\right) \\
&+\begin{bmatrix} A_{12}\left(\frac{\partial^2 u}{\partial x\partial y}+\frac{\partial w}{\partial x}\frac{\partial^2 w}{\partial x\partial y}\right) \\ +A_{11}\left(\frac{\partial^2 v}{\partial y^2}+\frac{\partial w}{\partial y}\frac{\partial^2 w}{\partial y^2}\right)\end{bmatrix}\left(\frac{\partial w}{\partial y}\right)
\end{aligned} \tag{28.7}
$$

$$
\begin{aligned}
Z_2 = {} & 2A_{66}\left(\frac{\partial u}{\partial y}+\frac{\partial v}{\partial x}+\frac{\partial w}{\partial x}\frac{\partial w}{\partial y}\right)\frac{\partial^2 w}{\partial x\partial y} \\
& +A_{66}\left(\frac{\partial^2 u}{\partial x\partial y}+\frac{\partial^2 v}{\partial x^2}+\frac{\partial w}{\partial y}\frac{\partial^2 w}{\partial x^2}+\frac{\partial w}{\partial x}\frac{\partial^2 w}{\partial x\partial y}\right)\frac{\partial w}{\partial y} \\
& +A_{66}\left(\frac{\partial^2 u}{\partial y^2}+\frac{\partial^2 v}{\partial x\partial y}+\frac{\partial w}{\partial y}\frac{\partial^2 w}{\partial x\partial y}+\frac{\partial w}{\partial x}\frac{\partial^2 w}{\partial y^2}\right)\frac{\partial w}{\partial x}
\end{aligned} \tag{28.8}
$$

The piezoelectric effect is presumed to be zero in this instance ($\phi = 0$) in the plates' borders; consequently.

3. Solving method

3.1 Discretization on the space domain

Examining the resonance of plates and plates is typically done using the GDQM, which is a common approach. The mth derivative of the displacement will be derived as follows.:

$$\frac{\partial^m f(x)}{\partial x^m} = \sum_{k=1}^{n} C_{ik}^{(m)} f(x) \tag{30}$$

Furthermore, the Kronecker item ($\otimes$), commonly referred to the partial derivative of two input variables, f (x,y), would've been expressed as detailed in the x and y contexts:

$$\frac{\partial^{m+n} f(x,y)}{\partial x^m \partial y^n (x,y)} = \left(C_y^{(n)} \otimes C_x^{(m)}\right) f(x,y) \tag{31}$$

In which m and n, correspondingly, Indicate the grid coordinates on the x and y axis of the system. The GDQM nodes could be expressed as follows when utilizing the Chebyshev-Gauss-Lobatto cosine format grid distribution model:

$$
\begin{aligned}
x_i &= \frac{a}{2}\left(1-\cos\left(\frac{(i-1)}{(m-1)}\pi\right)\right) i = 1,2,3,\ldots,m \\
y_i &= \frac{b}{2}\left(1-\cos\left(\frac{(j-1)}{(n-1)}\pi\right)\right) j = 1,2,3,\ldots,n
\end{aligned} \tag{32}
$$

By utilizing the derivatives of discretized shapes in the equations, the expression may take the following form:

$$[K_L + K_{NL}]d + [M]\ddot{d} = 0 \tag{33}$$

In which $\ddot{d}$ symbolizes the second time-dependent differentiation. Besides that, the both nonlinear and linear stiffness matrix designate by K_{NL} and K_L correspondingly thus the mass matrix is denoted by M. Each of the afore mentioned matrix are in $6N_xN_y \times 6N_xN_y$ dimension.

3.2 Derivation of Duffing-type equations

By inserting the $d^*=d.e^{i\omega}$ into Eq. (33), the eigen platform would have been expressed as:

$$([K_L + K_{NL}] - \omega^2[M])\{d\} = 0 \tag{34}$$

And *d* is obtained as:

$$\{d\} = \{u, v, w, \psi_x, \psi_y, \phi\}^T \tag{35}$$

The eigenvalue and eigenvector (w^*_{max}) are identified from the equations mainly by ignoring the K_{NL} (nonlinear stiffening matrix) Eq. (28). A recent eigenvalue/vector can be derived from the nonlinear eigenvalue system following the calculation of (K_{NL}), even by employing (K_L) as per Eq. (32). After each iteration, the difference between both the eigenvalues calculated from the prior incarnation and the one being iterated upon is checked to ensure that it falls under 1e-4.

$$|[K_L + K_{NL}] - \omega^2[M]| = 0 \tag{36}$$

4. Analytical results

The proposed FG-GOA core with SPHNC layers has potential practical applications in Aerospace and railway structural engineering and mechanical structures, vibration control devices, adaptive engineering components, and smart electronic systems. Its unique combination of a negative Poisson's ratio core and multi-scale hybrid nanocomposite layers enables lightweight, high-strength, and tunable dynamic responses, making it suitable for advanced structural and smart material applications. Throughout this section, you will find the charts and tables you need to identify the nonlinear dynamic investigation of the smart plate equipped via multiple BC.s .Table 1 details the geometry and electromechanical characteristics of the FG-GOA metamaterials and SPHNC plate.

5. Conclusions and analysis

5.1 Validation

In Table 2, we see a study of the resonant frequency of a rectangular plate via different B.C.s, and for different aspect ratios. Demonstrates the current research matches well with the findings of Ebrahimi and Dabbagh (2020). Table 3 shows the numerical outputs of another study, this time

Table 1 A material property of SPHNC and FG-GOA

SPHNC			
Property	Polyvinylidene fluoride	Property	Graphene
c_{11} (GPa)	238.24	E(GPa)	985
c_{22}	23.6	e_{31} (Cm^{-2})	-0.221
c_{33}	10.64	e_{33}	0.221
c_{13}	2.19	e_{15}	-0.221
c_{23}	1.92	s_{33} $(10^{-12}C^2m^{-2}N^{-1})$	1.106
c_{12}	3.98	ρ (kgm^{-3})	800
c_{55}	4.4	v	0.186
c_{66}	6.43	l (nm)	3
e_{31} (Cm^{-2})	-0.13	w (nm)	1.8
e_{33}	-0.276	h (nm)	0.7
e_{15}	-0.135	Properties	Carbon
s_{11} $(10^{-12}C^2m^{-2}N^{-1})$	110.67	E(GPa)	23.1
s_{33}	106.07	ρ (kgm^{-3})	1750
ρ (kgm^{-3})	1780	v	0.2
GOA			
Property	Gr	Property	Cu
E (GPa)	929.57	E (GPa)	65.789
ρ (kgm^{-3})	0.220	ρ (kgm^{-3})	8800
v	1800	v	0.387
α $(10^{-6}K^{-1})$	-3.98	α $(10^{-6}K^{-1})$	16.51
l (nm)	8.376	t (nm)	0.34

Table 2 Comparison of $\frac{\omega_{nl}}{\omega_l}$ of [0◦/90◦/90◦/0◦] symmetric laminated plate (R_1= R_2=∞)

B.C	CCCC		SSSS		SCSC	
h/b	Ebrahimi and Dabbagh (2020)	Present	Ebrahimi and Dabbagh (2020)	Present	Ebrahimi and Dabbagh (2020)	Present
0.001	35.98	36.47	19.74	20.38	28.95	29.47
0.1	32.49	33.33	19.06	19.75	26.65	27.41
0.2	26.46	27.64	17.43	18.18	22.32	23.32

Table 3 Analysis of the isotropic plate's nonlinear frequency relation ω_{nl}/ω_l compared to that of a B.C.s

w/h	Chu and Herrmann (1956)	Sundararajan *et al.* (2005)	Liu *et al*. (2016)	Balamurugan *et al*. (1969)	Present
0.2	1.0260	1.0256	1.0267	1.0254	1.0273
0.4	1.1003	1.0992	1.1013	1.0982	1.1041
0.6	1.2140	1.2126	1.2118	1.2119	1.2187
0.8	1.3574	1.3566	1.3467	1.3558	1.3591
1.0	1.5219	1.5234	1.4987	1.5200	1.5164

looking at the relation ω_{nl}/ω_l of the rectangular plate via different B.C.s and shaking amplitudes (*w*max=*w/h*).

This verification shows that this study agrees very well with Sundararajan *et al*. (2005), Chu and Herrmann (1956), Liu *et al*. (2016) and Balamurugan *et al*. (1969).

5.2 Figures

Fig.2 displays the impact of (h_{SPHNC}) on the ratio (ω_{nl}/ω_l) and (ω_{nl}.) via raising the dimensionless amplitude from 0.1 to 1, the ratio (ω_{nl}/ω_l) and (ω_{nl}) are both enhanced, as shown in Fig. 2. In which the (h_{SPHNC}) is raised from 0.025 to 0.1 in both clamped and simply supported B.C.s, There's an obvious rise in (ω_{nl}/ω_l) and ω_{nl}. As expected, the ratio of (ω_{nl}/ω_l) under simply supported B.C. is greater than under clamped boundary conditions.

Fig. 3 illustrates the correlation between the GOA core thickness and the smart plate's (ω_{nl}/ω_l) and (ω_{nl}) values. As

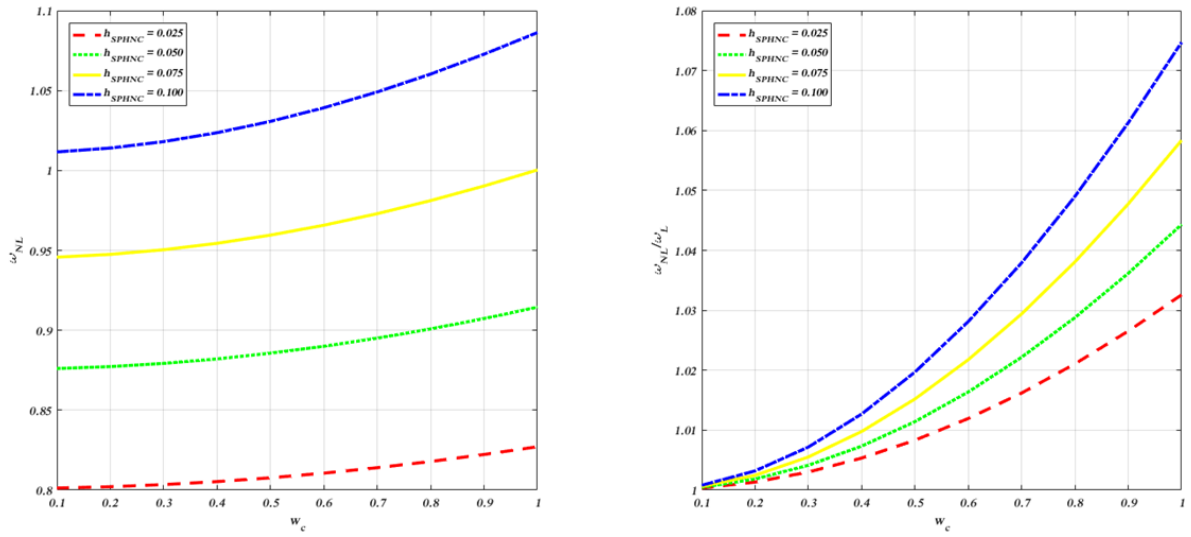

(a) C-C-C-C

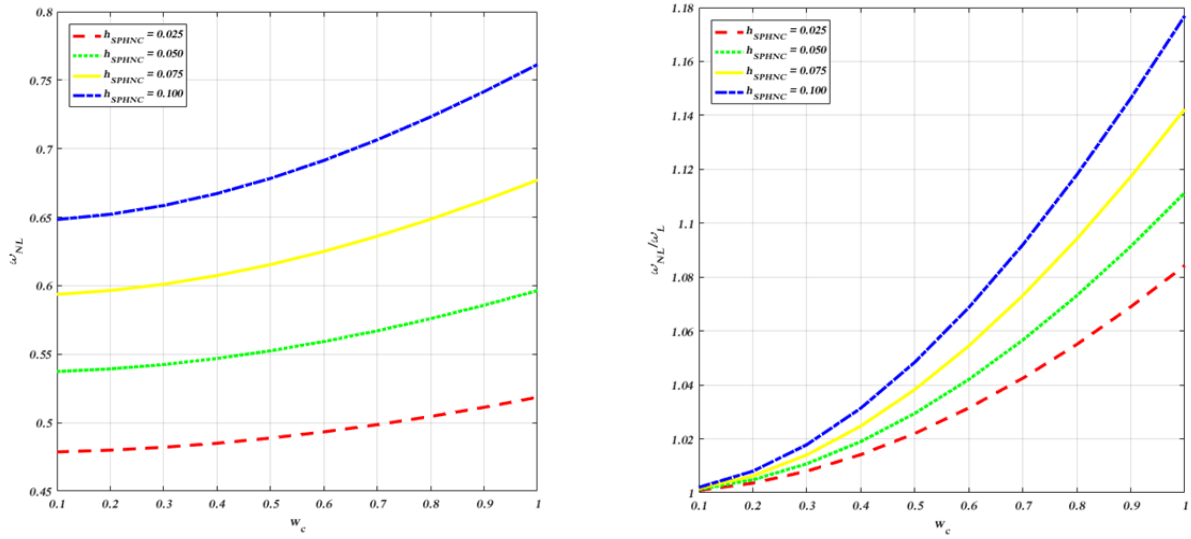

(b) S-S-S-S

Fig. 2 The impact of variations in SPHNC layers thickness (h_{SNC}) on the ratio (ω_{nl}/ω_l) and the ω_{nl} of the composite plate under different B.C.s

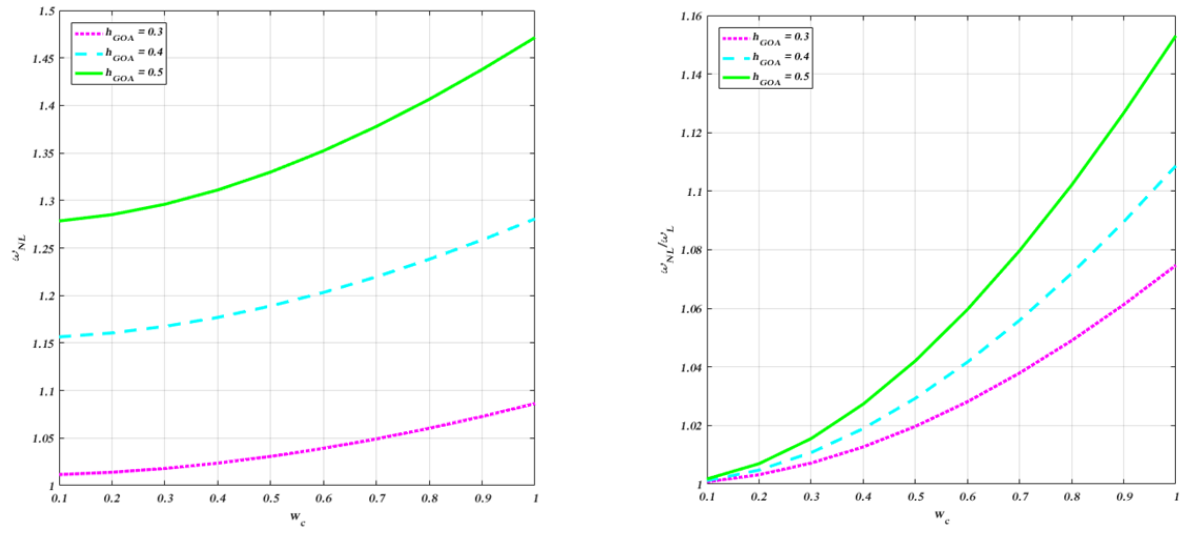

(a) S-S-S-S

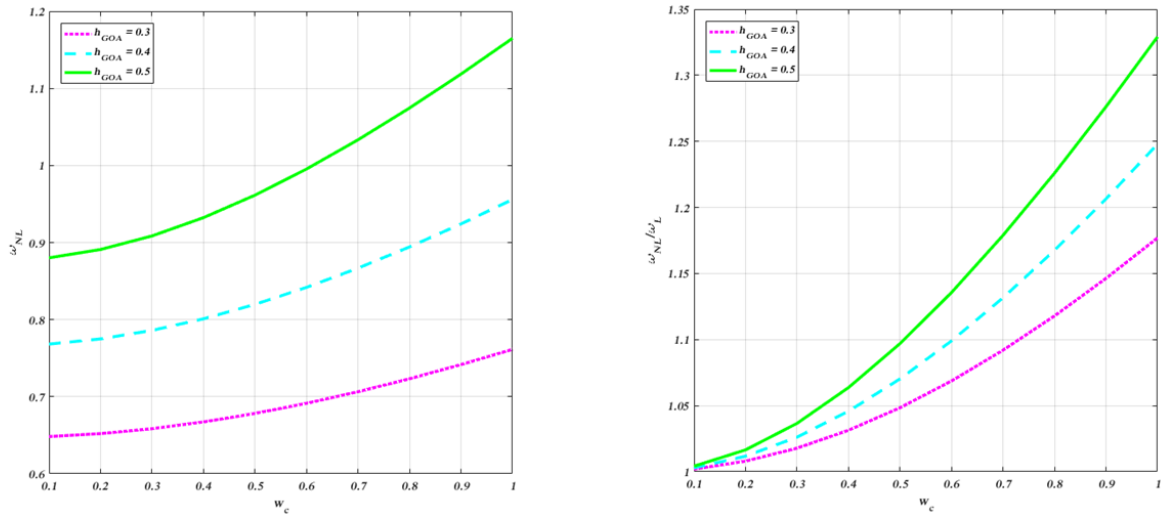

(b) S-S-S-S

Fig. 3 The impact of different thicknesses of GOA (h_{GOA}) on the ratio (ω_{nl}/ω_l) and (ω_{nl}) of the composite plate under different B.C.s

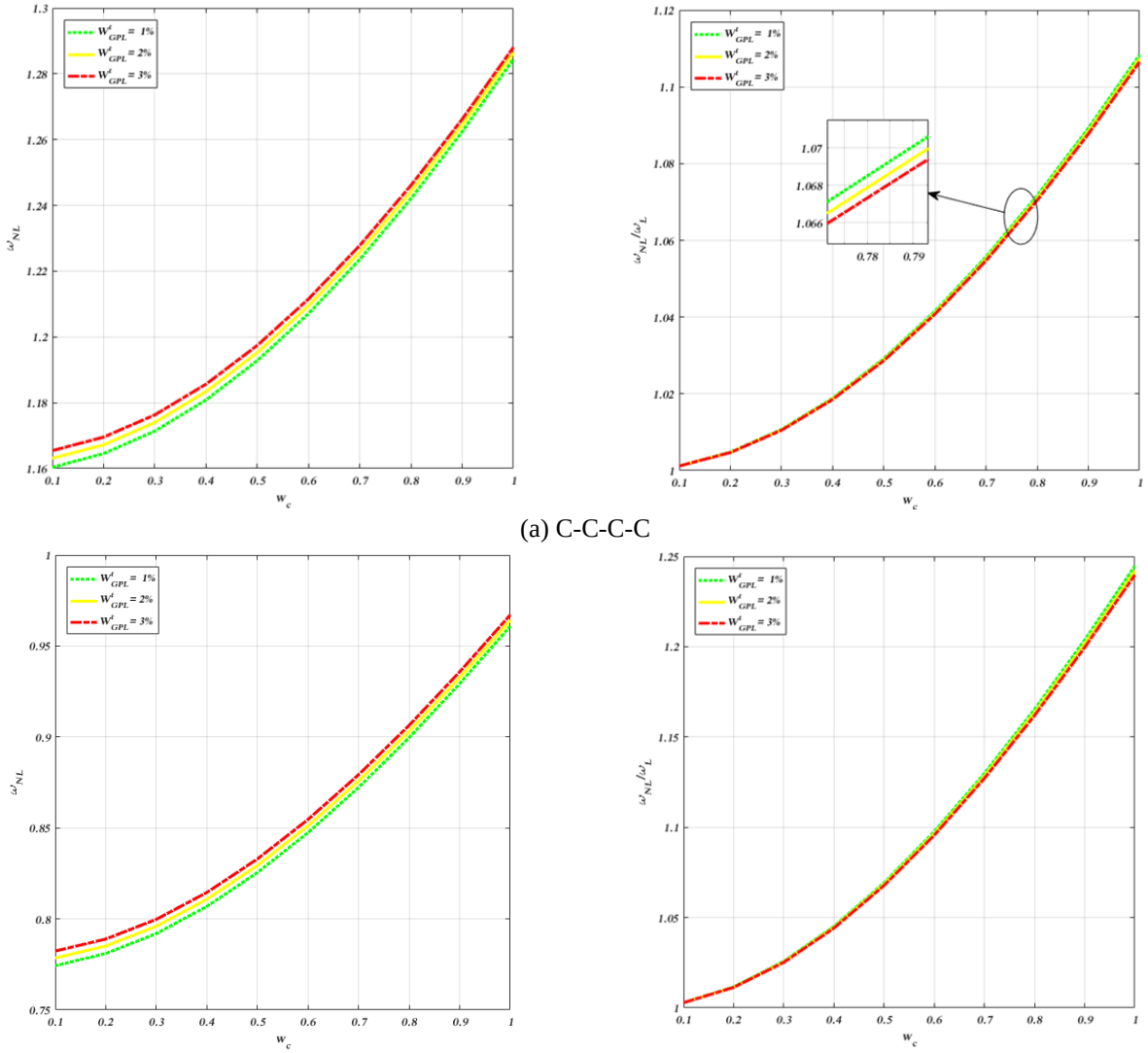

(a) C-C-C-C

(b) S-S-S-S

Fig. 4 The impact of varied weight portion of graphene nanoplatelets ($\boldsymbol{W_{GR}}$) on the (ω_{nl}/ω_l) and (ω_{nl}) of the composite plate under different B.C.s

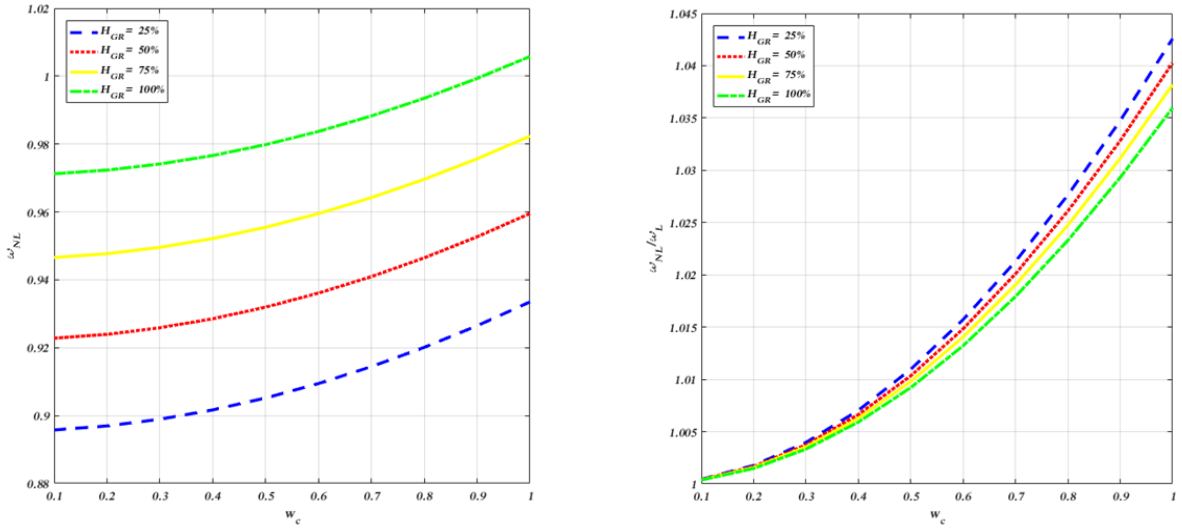

(a) C-C-C-C

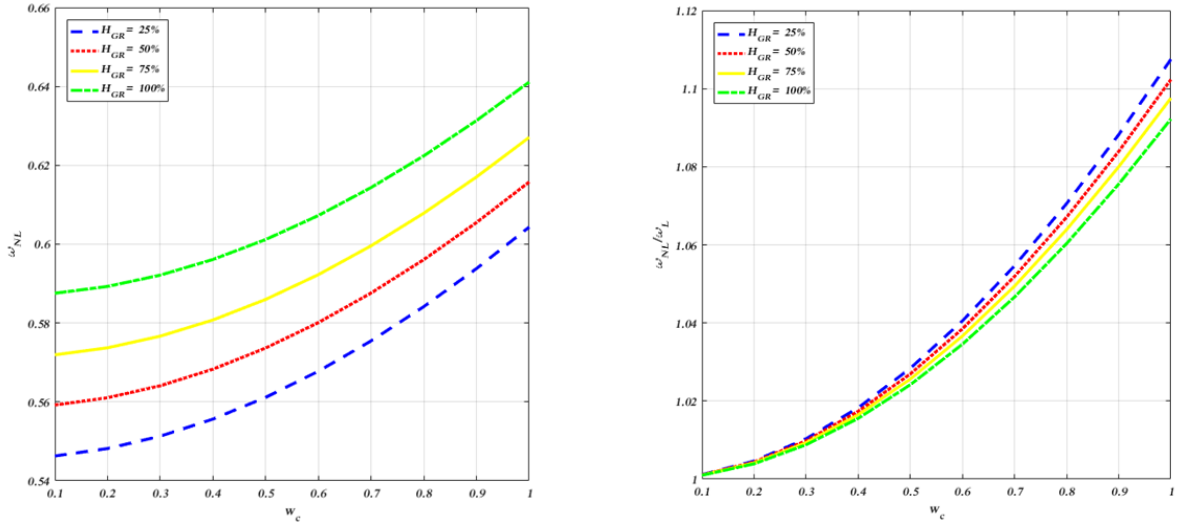

(b) S-S-S-S

Fig. 5 The impact of various angles of GOA folding degree ($\boldsymbol{H_{GR}}$) on the (ω_{nl}) of the composite plate under two different B.C.s

illustrated in Fig. 3, when the magnitude (*w*max) is raised from 0.1 to 1, both (ω_{nl}/ω_l) and (ω_{nl}) expand. In addition, by raising the GOA core thickness, both (ω_{nl}/ω_l) and (ω_{nl}) are higher than their previous. In comparison to simply supported B.C., clamped has a lessened (ω_{nl}/ω_l) value.

Fig. 4 displays how (ω_{nl}/ω_l) and (ω_{nl}) of the composite plate change as a function of W_{GR}. Fig. 4 demonstrates that increasing the domain from 0.1 to 1 result in larger values for both (ω_{nl}/ω_l) and (ω_{nl}). As can be seen, both clamped and simply supported B.C.s experience increases in (ω_{nl}/ω_l) as raised from 1% to 3%. The (ω_{nl}/ω_l) in clamped can be calculated to be smaller than that of simply supported B.C.s, which is a notable finding.

Fig. 5 illustrates the impact that H_{GR} has (ω_{nl}/ω_l) and (ω_{nl}) have on the SPHNC plate. According to what is presented in Fig. 5, (ω_{nl}/ω_l) and (ω_{nl}) are raised by elevating the maximum value of the magnitude from 0.1 to 1. Additionally, by decreasing the inclination of H_{GR}, (ω_{nl}) can be made smaller. It is plain to see that there are fewer (ω_{nl}/ω_l) in simply supported boundary conditions than there are in clamped ones.

Fig. 6 shows how SPHNC plate's (ω_{nl}/ω_l) and (ω_{nl}) are affected by the carbon fiber volume percentage. As can be seen in Fig. 6, both (ω_{nl}/ω_l) and (ω_{nl}) has increased in size due to the rise in (*w*max) from 0.1 to 1. The ratio (ω_{nl}/ω_l) evidently boosts as theCF value diminishes from 0.3 to 0.1 i n both the clamped and simply supported B.C.s. It is easily observable and verifiable that the magnitude of (ω_{nl}/ω_l) in clamped is lower than that of simply supported B.Cs.

It is clear from looking at Fig. 7 that the pore size constant, e_0, has an effect on the (ω_{nl}/ω_l) and also (ω_{nl}) of the smart GOA plate. As illustrated in Fig. 7, (ω_{nl}/ω_l) is raised by elevating the maximum value of the magnitude (*w*max) from 0.1 to 1. When (e_0) increases from 0.1 to 0.5 in both clamped and simply supported B.C.s, there's an apparent rise in the value of (ω_{nl}/ω_l). It has come to the attention that (ω_{nl}/ω_l) in clamped one is significantly less than it was in simply supported boundary condition.

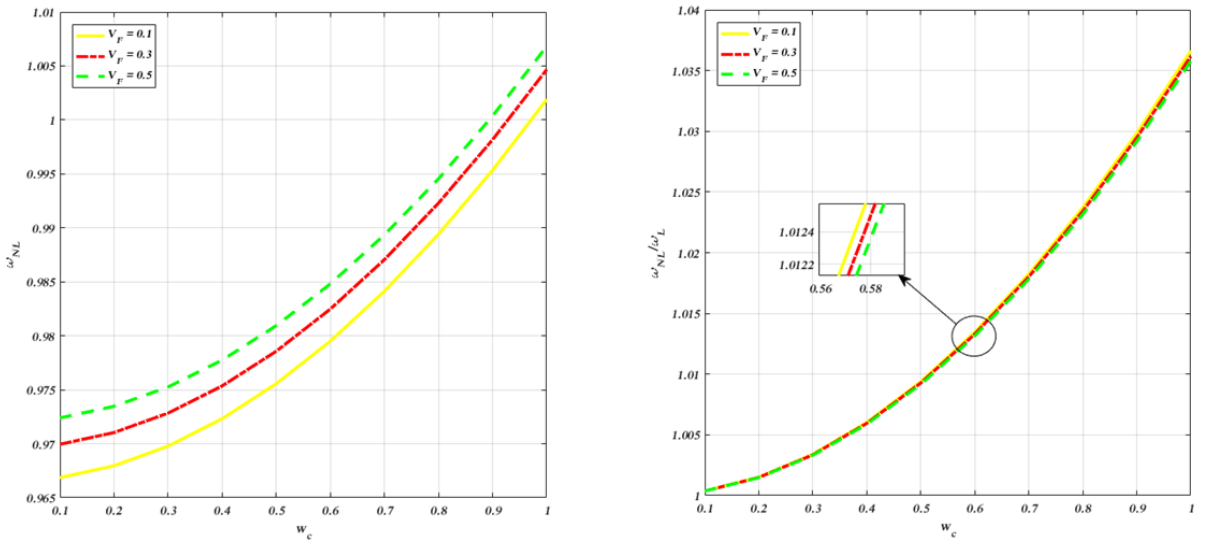

(a) C-C-C-C

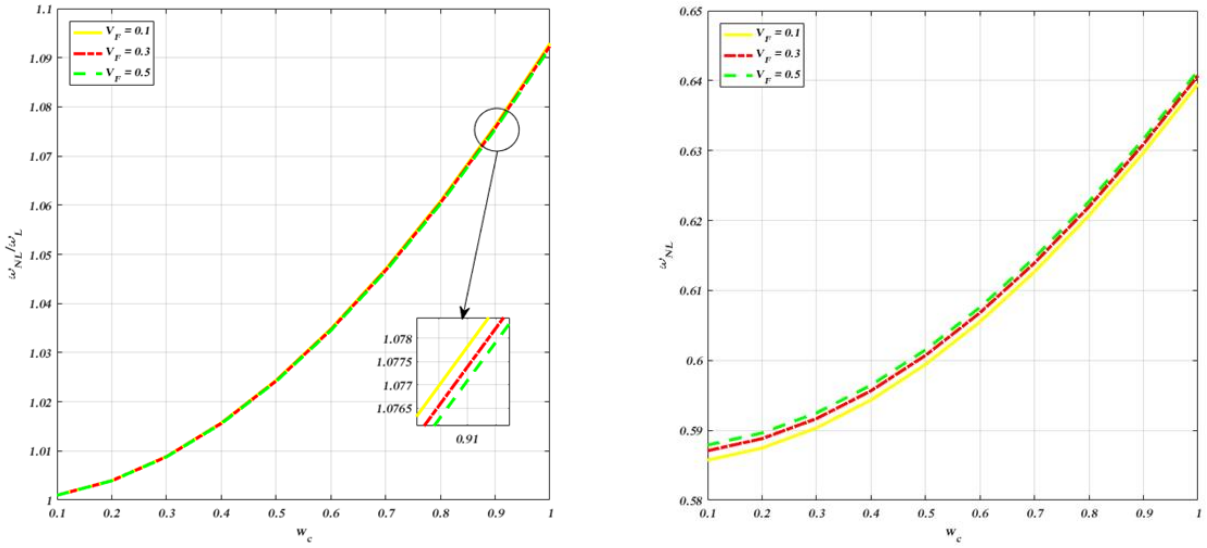

(b) S-S-S-S

Fig. 6 The impact of different volume fractions of fibers ($\boldsymbol{V_F}$) on (ω_{nl}/ω_l) and (ω_{nl}) of the composite plate under different B.C.s

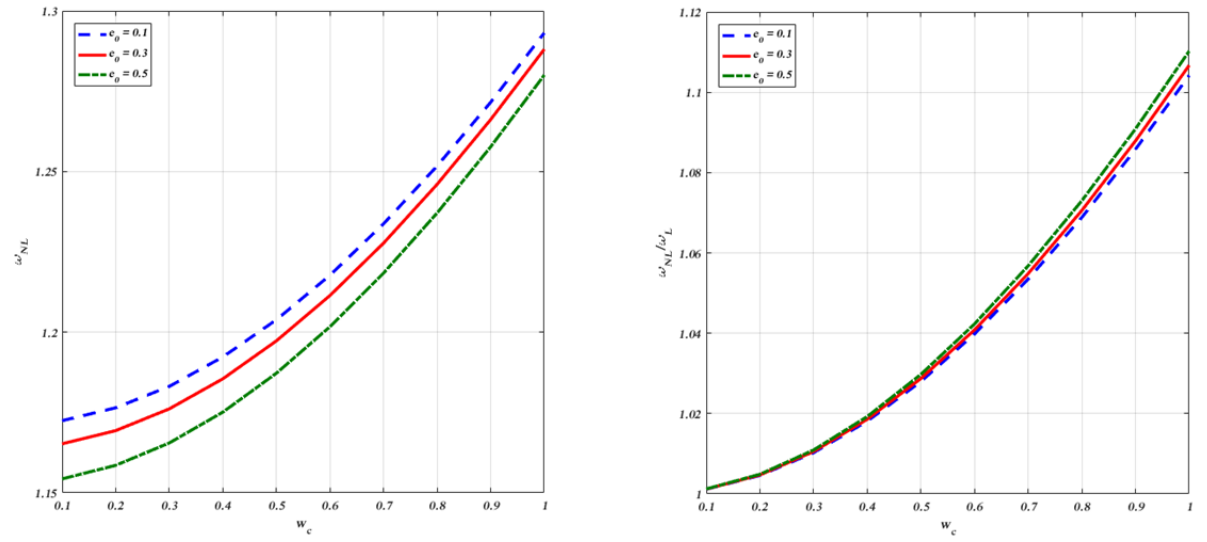

(a) C-C-C-C

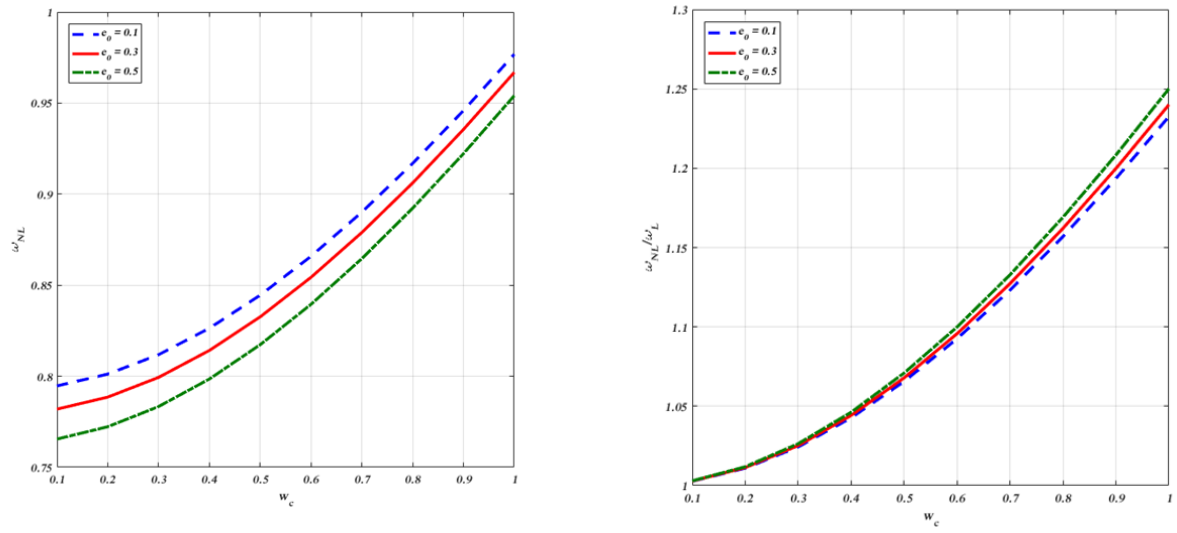

(b) S-S-S-S

Fig. 7 The impact of varied porosity constant (e_0) on (ω_{nl}/ω_l) and (ω_{nl}) of the composite plate under two different boundary conditions

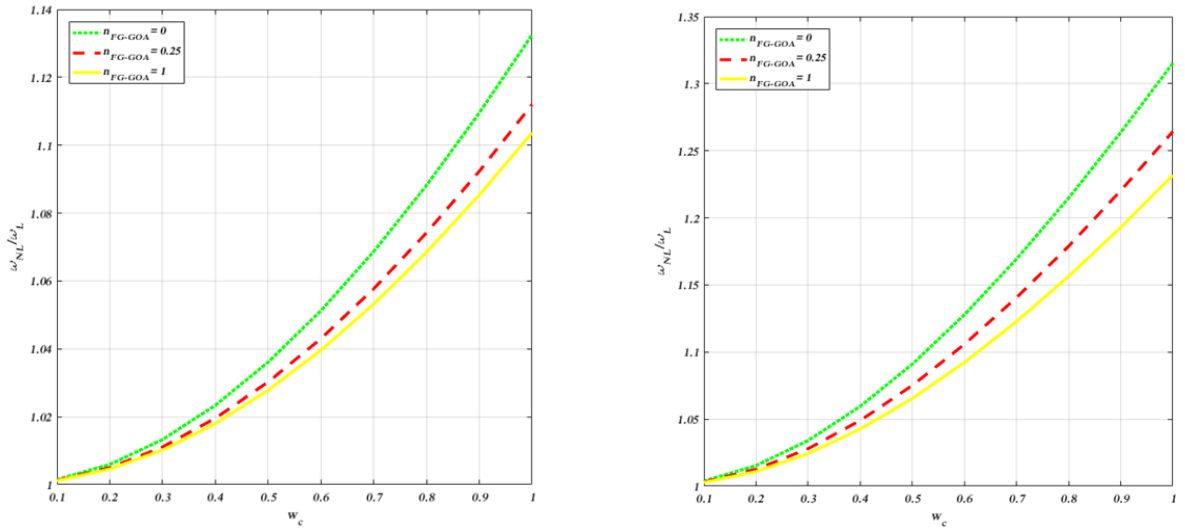

(a) C-C-C-C (b) S-S-S-S

Fig. 8 The impact of varied FG power index ($n_{FG\text{-}GOA}$) on (ω_{nl}/ω_l) and (ω_{nl}) of the composite plate under various boundary conditions

Fig. 8 shows how (ω_{nl}/ω_l) of the smart hybrid FG-GOA plate changes when the ($n_{FG\text{-}GOA}$) of is changed. According to the information shown in Fig. 8, (ω_{nl}/ω_l) grows as the domain ($w$max) raised from 0.1 to 1. In addition, increasing the FG-GOA ($n_{FG\text{-}GOA}$) (from 0 to 1) decreased (ω_{nl}/ω_l) in clamped and simply supported B.C. The amount of (ω_{nl}/ω_l) in clamped is noticeably smaller than in simply supported B.C.

The present approach offers advantages over traditional methods by accurately capturing nonlinear vibrations, porosity effects, and multi-scale interactions in FG-GOA/ SPHNC plates using HSDT and GDQM. Its main limitation is higher computational complexity and the need for detailed material characterization, but it provides a more comprehensive understanding of the dynamic behavior of advanced smart hybrid nanocomposite plates.

6. Conclusions

The novelty of the present research lies in the investigation of nonlinear vibrations of a piezoelectric sandwich plate combining a FG graphene origami auxetic core with smart porous multi-scale hybrid nanocomposite layers. This unique configuration, integrating negative Poisson's ratio behavior with multi-scale reinforcement, has not been studied before and provides new insights into tunable dynamic responses of advanced smart structures. In this paper, HSDT is used to investigate the nonlinear oscillation dynamics of electromechanical composite plates. A FG-GOA core and SPHNC layers make up the composite plate's substance layers. Effective properties of the SPHNC layer is a direct consequence of HT and ROM models. The sandwich plate's nonlinear equations and related B.C.s are

obtained. Once this is done, GDQM is used to compute the nonlinear governing equations. The current definition of an outcomes review could be as follows:

• Raising the weight proportion of GPL and their resonance amplitude raises the nonlinear frequency ratio.

• By raising the same exterior voltage and porosity and the porous SPHNC layer thicknesses, (ω_{nl}/ω_l) is enhanced.

• Increasing the FG-GOA power index decreased (ω_{nl}/ω_l) in clamped and simply supported boundary conditions.

• The amount of (ω_{nl}/ω_l) in clamped is noticeably smaller than in simply supported B.C.

References

Asghari, M. and Taati, E. (2013), "A size-dependent model for functionally graded micro-plates for mechanical analyses", *J. Vib. Control*, **19**(1614-1632). https://doi.org/10.1177/1077546312442563.

Balamurugan, V., Ganapathi, M. and Varadan, T.K. (1996), "Nonlinear dynamic instability of laminated composite plates using finite element method", *Comput. Struct.*, **60**(1), 125-130. https://doi.org/10.1016/0045-7949(95)00368-1

Chen, D., Yang, J. and Kitipornchai, S. (2017), "Nonlinear vibration and postbuckling of functionally graded graphene reinforced porous nanocomposite beams", *Compos. Sci. Technol.*, **145**(102-112). https://doi.org/10.1016/j.compscitech.2017.02.008.

Chen, J. and Li, Q.S. (2017), "Nonlinear aeroelastic flutter and dynamic response of composite laminated cylindrical shell in supersonic air flow", *Compos. Struct.*, **168**(474-484). https://doi.org/10.1016/j.compstruct.2017.02.019.

Chu, H.N. and Herrmann, G. (1956), "Influence of large amplitudes on free flexural vibrations of rectangular elastic plates", *J. Appl. Mech.*, **23**(4), 309-315. https://doi.org/10.1115/1.4011396

Ebrahimi, F. (2024), *Mechanics of Auxetic Materials and Structures*, CRC Press, Boca Raton, FL, U.S.A.

Ebrahimi, F. and Barati, M.R. (2016a), "A nonlocal higher-order refined magneto-electro-viscoelastic beam model for dynamic analysis of smart nanostructures", *Int. J. Eng. Sci.*, **107**(183-196). https://doi.org/10.1016/j.ijengsci.2016.08.001.

Ebrahimi, F. and Barati, M.R. (2016b), "Buckling analysis of nonlocal third-order shear deformable functionally graded piezoelectric nanobeams embedded in elastic medium", *J. Brazil. Soc. Mech. Sci. Eng.*, **38**(1-10). https://doi.org/10.1007/s40430-016-0551-5.

Ebrahimi, F. and Dabbagh, A. (2017), "On flexural wave propagation responses of smart FG magneto-electro-elastic nanoplates via nonlocal strain gradient theory", *Compos. Struct.*, **162**(281-293). https://doi.org/10.1016/j.compstruct.2016.11.058.

Ebrahimi, F. and Dabbagh, A. (2019), *Wave Propagation Analysis of Smart Nanostructures*, CRC Press, Boca Raton, FL, U.S.A.

Ebrahimi, F. and Dabbagh, A. (2020), *Mechanics of Nano-composites: Homogenization and Analysis*, CRC Press, Boca Raton, FL, U.S.A.

Ebrahimi, F. and Rastgoo, A. (2009), "Nonlinear vibration of smart circular functionally graded plates coupled with piezoelectric layers", *Int. J. Mech. Mater. Des.*, **5**(157-165). https://doi.org/10.1007/s10999-008-9091-1.

Ebrahimi, F. and Reza Barati, M. (2016c), "Magnetic field effects on buckling behavior of smart size-dependent graded nanoscale beams", *Eur. Phys. J. Plus*, **131**(245). https://doi.org/10.1140/epjp/i2016-16238-8.

Ebrahimi, F. and Zia, M. (2015), "Large amplitude nonlinear vibration analysis of functionally graded Timoshenko beams with porosities", *Acta Astronaut.*, **111**(16-25). https://doi.org/10.1016/j.actaastro.2015.06.014.

Flamourakis, G., Spanos, I., Vangelatos, Z., Manganas, P., Papadimitriou, L. and Grigoropoulos, C. (2020), "Laser-made 3D auxetic metamaterial scaffolds for tissue engineering applications", *Macromol. Mater. Eng.*, **305**(1-9). https://doi.org/10.1002/mame.202000238.

Ghorbanpour Arani, A., Jamali, M., Ghorbanpour-Arani, A.H., Kolahchi, R. and Mosayyebi, M. (2017), "Electro-magneto wave propagation analysis of viscoelastic sandwich nanoplates considering surface effects", *Proc. Inst. Mech. Eng. Part C J. Mech. Eng. Sci.*, **231**(387-403). https://doi.org/10.1177/0954411916688994.

Hosseini, M., Mahinzare, M. and Ghadiri, M. (2018), "Magnetic field effect on vibration of a rotary smart size-dependent two-dimensional porous functionally graded nanoplate", *J. Sound Vib.*, **431**(51-65). https://doi.org/10.1177/1045389X18781034.

Ilkhani, M.R. and Hosseini-Hashemi, S.H. (2016), "Size dependent vibro-buckling of rotating beam based on modified couple stress theory", *Compos. Struct.*, **143**(75-83). https://doi.org/10.1016/j.compstruct.2016.02.013.

Jafari, A.A., Khalili, S.M.R. and Tavakolian, M. (2014), "Nonlinear vibration of functionally graded cylindrical shells embedded with a piezoelectric layer", *Thin Walled Struct.*, **79**(8-15). https://doi.org/10.1016/j.tws.2014.01.030.

Jiang, L. and Hu, H. (2017), "Low-velocity impact response of multilayer orthogonal structural composite with auxetic effect", *Compos. Struct.*, **169**(62-68). https://doi.org/10.1016/j.compstruct.2016.10.018.

Liu, C., Ke, L.L., Yang, J. and Kitipornchai, S. (2016), "Nonlinear vibration of piezoelectric nanoplates using nonlocal Mindlin plate theory", *Mech. Adv. Mater. Struct.*, **23**(6), 6494-6504. https://doi.org/10.1080/15376494.2016.1149648.

Mahinzare, M., Ranjbarpur, H. and Ghadiri, M. (2018), "Free vibration analysis of a rotary smart two directional functionally graded piezoelectric material in axial symmetry circular nanoplate", *Mech. Syst. Signal Proc.*, **100**(188-207). https://doi.org/10.1016/j.ymssp.2017.09.063.

Mahinzare, M., Rastgoo, A. and Ebrahimi, F. (2024a), "On nonlinear vibration of piezo-electrically multiscale hybrid nanocomposite sandwich plate including an auxetic core based on HSDT", *Int. J. Struct. Stabil. Dyn.*, **24**(5). https://doi.org/10.1142/S0219455424500824.

Mahinzare, M., Rastgoo, A. and Ebrahimi, F. (2024b), "On nonlinear vibration of piezo-electrically multiscale hybrid nanocomposite sandwich plate including an auxetic core based on HSDT", *Int. J. Struct. Stabil. Dyn.*, **24**(5), 2450069. https://doi.org/10.1142/S021945542450069X

Malekzadeh, P. (2008), "Differential quadrature large amplitude free vibration analysis of laminated skew plates based on FSDT", *Compos. Struct.*, **83**(189-200). https://doi.org/10.1016/j.compstruct.2007.04.007.

Mangalasseri, A.S., Mahesh, V., Mukunda, S., Mahesh, V., Ponnusami, S.A., Harursampath, D. and Tounsi, A. (2023), "Vibration based energy harvesting performance of magneto-electro-elastic beams reinforced with carbon nanotubes," *Adv. Nano Res.*, **14**(1), 27-43. https://doi.org/10.12989/anr.2023.14.1.027

Nguyen, D.D. and Pham, C.H. (2018), "Nonlinear dynamic response and vibration of sandwich composite plates with negative Poisson's ratio in auxetic honeycombs", *J. Sandw. Struct. Mater.*, **20**(692-717). https://doi.org/10.1177/1099636216674729.

Quan, T.Q., Anh, V.M., Mahesh, V. and Duc, N.D. (2020),

"Vibration and nonlinear dynamic response of imperfect sandwich piezoelectric auxetic plate", *Mech. Adv. Mater. Struct*., 1-11. https://doi.org/10.1080/15376494.2020.1752864.

Rachid, E.K., Khalid, E.B. and Rhali, B. (2014), "A semi-analytical study of geometrically nonlinear free axisymmetric vibrations of thin circular functionally graded plates using iterative and explicit analytical solution", *Appl. Mech. Mater*., **704**(131-136). https://doi.org/10.4028/www.scientific.net/AMM.704.131.

Sadeghzadeh, S. and Mahinzare, M. (2020), "Nonlocal strain gradient theory for dynamical modeling of a thermo-piezo-magnetically actuated spinning inhomogeneous nanoshell", *Mech. Based Des. Struct*., **48**(1-22). https://doi.org/10.1080/15397734.2020.1766495.

Sh, E.L., Kattimani, S. and Vinyas, M. (2022), "Nonlinear free vibration and transient responses of porous functionally graded magneto-electro-elastic plates", *Arch. Civ. Mech. Eng*., **22**(1-26). https://doi.org/10.1007/s43369-022-00539-6.

Shariyat, M., Khaghani, M. and Lavasani, S.M.H. (2010), "Nonlinear thermoelasticity, vibration, and stress wave propagation analyses of thick FGM cylinders with temperature-dependent material properties", *Eur. J. Mech. A Solids*, **29**(378-391). https://doi.org/10.1016/j.euromechsol.2009.10.007.

Shen, H.S. and Xiang, Y. (2014), "Nonlinear vibration of nanotube-reinforced composite cylindrical panels resting on elastic foundations in thermal environments", *Compos. Struct*., **111**(291-300). https://doi.org/10.1016/j.compstruct.2014.02.016.

Shruti, M., Hemanth, N.S., Badgayan, N.D. and Sahu, S.K. (2020), "Compressive behavior of auxetic structural meta-material for lightweight construction using ANSYS static structural analysis", *Mater. Today Proc*., **38(**12-17). https://doi.org/10.1016/j.matpr.2020.05.410.

Sofiyev, A.H. (2016), "Nonlinear free vibration of shear deformable orthotropic functionally graded cylindrical shells", *Compos. Struct*., **142**(35-44). https://doi.org/10.1016/j.compstruct.2016.01.081.

Sundararajan, N., Prakash, T. and Ganapathi, M. (2005), "Nonlinear free flexural vibrations of functionally graded rectangular and skew plates under thermal environments", *Finite Elem. Anal. Des.*, **42**(152-168). https://doi.org/10.1016/j.feades.2005.04.005.

Wang, Z., Zulifqar, A. and Hu, H. (2016), "Auxetic composites in aerospace engineering", *Adv. Compos. Mater. Aerosp. Eng*., 213-240. https://doi.org/10.1016/b978-0-08-100037-3.00007-9.

Yang, W., Li, Z.M., Shi, W. and Xie, B.H. (2004), "On auxetic materials", *J. Mater. Sci*., **39**(3269-3279). https://doi.org/10.1023/B:JMSC.0000026928.93231.e0.

Zhang, W., Zhao, S., Scarpa, F., Wang, J. and Sun, R. (2021), "In-plane mechanical behavior of novel auxetic hybrid meta-materials", *Thin Walled Struct*., **159**(107191). https://doi.org/10.1016/j.tws.2020.107191.

CC